

# Twinning in GaAs nanowires on patterned GaAs(111)B

Thomas Walther<sup>1,2,\*</sup> and Andrey B. Krysa<sup>2,3</sup>

Received 25 May 2014, revised 31 July 2014, accepted 10 September 2014

Published online 8 October 2014

We have studied twinning in GaAs nanowires grown via holes in a silica mask deposited on GaAs(111)B substrates by metal-organic chemical vapour epitaxy without catalysts. Twins perpendicular to the growth direction form in the nanowires, their {111}-type side facets leading to corrugation of their {110} side walls. The top facets are almost atomically smooth. Aberration corrected annular dark-field scanning transmission electron microscopy reveals all twins are rotational, commencing with layers of Ga and finishing with As atoms. Energy-loss spectroscopic profiling has shown no significant changes in the band-gap or bulk plasmon energy at those twin boundaries, and the observed reduction of the interface plasmon energy by  $\sim 0.13$  eV is close to the detection limit of the technique, reflecting the very low energetic electronic changes related to twin formation.

## 1 Introduction

Nanowires of compound semiconductors often exhibit twinning during growth, e.g. in GaAs [1–5], GaP [6], GaSb [7], InAs [8] InP [9, 10] and ZnSe [11]. The optical properties of such wires are a function of their diameters [2] and the degree of twinning [4], both of which depend on a number of growth parameters in a complicated way [7].

Twin-free GaAs nanowires have been grown from gas phase epitaxy with the help of gold nanoparticles as catalysts [3] or by molecular beam epitaxy [5]. Here, we concentrate on the growth of highly uniform GaAs nanowires (with InGaAs inserts for optical spectroscopy) by metal-organic vapour phase epitaxy without using any catalysts.

{111} rotational twins in compound semiconductors implicate a transition of the local stacking sequence from cubic (sphalerite) to hexagonal (wurtzite). This microstructural change has direct implications on the electronic structure and therefore also the optical properties. For gallium nitride (GaN) and related alloys, where the wurtzite structure is more common, the bandgap

of the hexagonal structure is generally reported to be  $\sim 0.2$  eV larger than the bandgap of the corresponding cubic structure [12–16], although one group initially reported the reverse based on cathodoluminescence studies [17, 18]. For GaAs, where the thermodynamically stable phase is cubic, the situation is more complicated because, firstly, the bandgaps of sphalerite and wurtzite structure are here even closer while the scatter of experimental and theoretical values remains large and, secondly, the hexagonal phase is often preferentially formed only in small nanowires [19] where additional quantum confinement effects need to be taken into account. The most recent studies indicate that the bandgap of hexagonal GaAs will be only 40–70 meV [20–22] larger than that of cubic GaAs, and *ab initio* calculations have shown an enormous scatter, cf. the overview in [20]. Hence, an interesting question that may be addressed by electron energy-loss spectroscopy (EELS) is whether a correlation can be made between the existence of twins and the local electronic structure as measured in the low-loss range.

## 2 Experimental

GaAs nanowires were fabricated by depositing 20 nm silica on a GaAs(111)B substrate. Electron beam lithography and reactive ion beam etching were then combined to pattern square arrays of  $25 \times 25$  holes, with pitches of 4  $\mu\text{m}$  and various diameters between 50 and 250 nm. After an anneal at 780°C in a hydrogen/arsine

\* Corresponding author: e-mail: t.walther@sheffield.ac.uk,  
Phone: +0044 114 222 5891, Fax: +0044 114 222 5143

<sup>1</sup> Kroto Centre for High-Resolution Imaging & Analysis, Department of Electronic & Electrical Engineering, University of Sheffield, Mappin Street, Sheffield S1 3JD, UK

<sup>2</sup> Semiconductor Materials & Devices Group, Department of Electronic & Electrical Engineering, University of Sheffield, Mappin Street, Sheffield S1 3JD, UK

<sup>3</sup> National Centre for III/V Technologies, Nanoscience and Technology Building, University of Sheffield, North Campus, Broad Lane, Sheffield S3 7HQ, UK

mixture, GaAs was grown catalyst-free at 750°C from trimethyl-gallium and arsine sources by low-pressure metal-organic vapour phase epitaxy. Halfway through the 10 minutes growth, trimethyl-indium was added for 2 s of growth to produce InGaAs quantum dots embedded within the wires. Finally, after a brief growth interrupt, a surface passivating GaAsP cap was grown by addition of phosphine for 10 s, which was maintained during ramping down the growth temperature to room temperature. More details of the growth and optical investigation by photoluminescence can be found in reference [23]. Figure 1 shows such a regular nanowire array at inclined and in top view, observed in a scanning electron microscope with secondary electron detector, demonstrating the achieved uniformity ( $\sim 99\%$  site coverage,  $3\text{--}5\ \mu\text{m}$  length,  $138 \pm 20\ \text{nm}$  diameter, where the ability to measure nanowire length and diameter is mainly limited by the viewing angle and the sampling of  $14\ \text{nm}/\text{pixel}$  in figure 1b, respectively) and the hexagonal cross-section of the nanowires, with  $\{110\}$ -type side facets.

The nanowires were then harvested from the GaAs substrate by scratching off one array with a sharp scalpel, and putting them onto a holey carbon film supported by a copper mesh for transmission electron microscopy.

Scanning Transmission Electron Microscopy (STEM) was performed using two different instruments, a JEOL 2010F at 197 kV, and a double aberration corrected JEOL Z3100 R005 operated in scan mode with  $\sim 0.1\ \text{nm}$  probe size and  $100\ \text{pA}$  beam current by using a  $28\ \text{mrad}$  semi-angle of convergence at  $300\ \text{kV}$  acceleration voltage and an increased extraction voltage of  $A1 = 2.1\ \text{kV}$  [24]. High-angle annular dark-field (HAADF) images were recorded with collection angles of  $\sim 55\ \text{mrad}$  (JEOL 2010F) or  $\sim 65\ \text{mrad}$  (JEOL R005), respectively. Both electron microscopes are equipped with Gatan Imaging Filters (GIFs) for electron energy-loss spectroscopy (EELS) and energy-filtered imaging; the JEOL 2010F with a GIF200 and the JEOL R005 with a GIF Tridium 865.

### 3 Results and discussion

Figure 2 demonstrates that the needles were preferentially broken at a position about half-way above the substrate, as their apparent lengths are reduced to  $\sim 2\ \mu\text{m}$ . The diameters determined agree well with the previous SEM measurements in figure 1. Some of the nanowires show a banded contrast typical for twin formation. An enlarged view of the end of such a needle is shown in the top part of figure 3, along with a diffraction pattern acquired from this needle, which is shown in the lower part of figure 3.

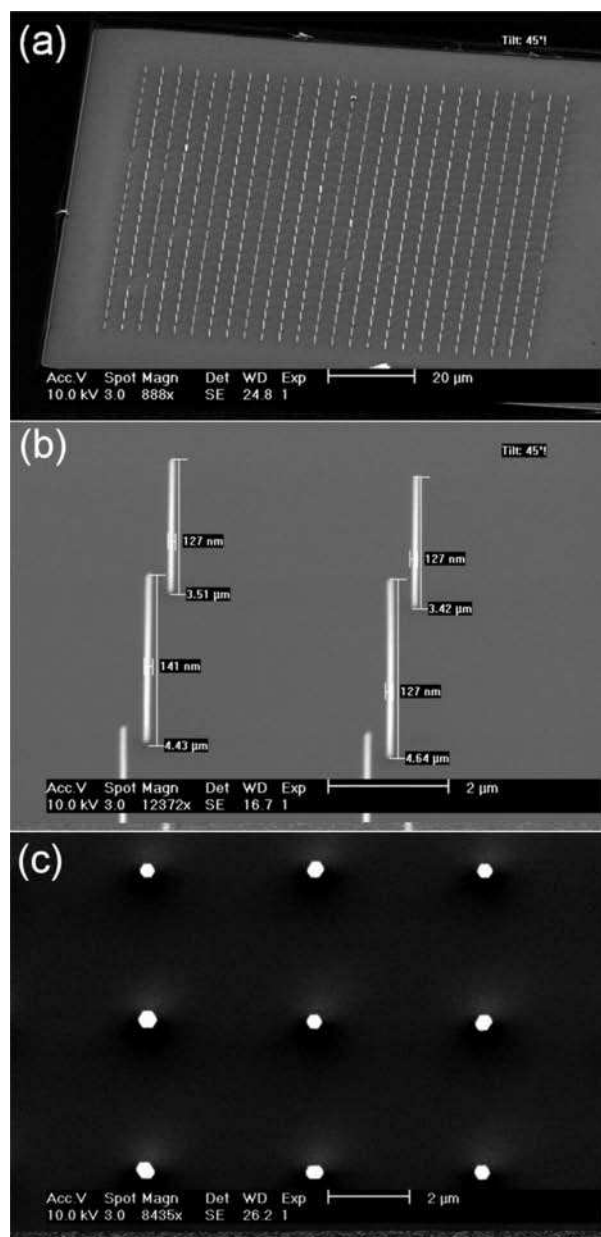
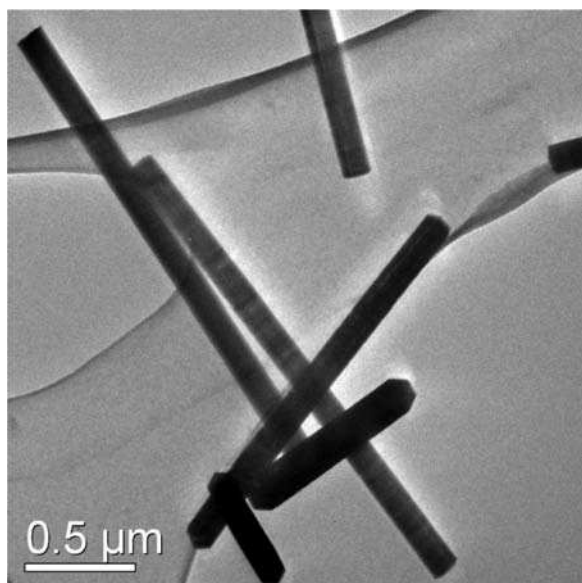


Fig. 1 Secondary electron imaging of a typical array of nanowires in a scanning electron microscope in side and top view. pitch:  $4\ \mu\text{m}$ , nominal hole mask diameter:  $0.1\ \mu\text{m}$ , sampling:  $190\ \text{nm}/\text{pixel}$  (a),  $14\ \text{nm}/\text{pixel}$  (b),  $20\ \text{nm}/\text{pixel}$  (c).

The diffraction pattern has been displayed in colour code to emphasise that some of the Bragg reflections are split. This is due to an almost periodic arrangement of the twins [6, 23] that are very dense: at an average spacing of only  $2.7\ \text{nm}$  (cf. histogram in figure 4) they make up  $\sim 10\%$  of the total nanowire volume.

The high-resolution electron microscopy (HREM) lattice images displayed in figure 5 show that the twins form



**Fig. 2** Bright field (BF) TEM image at 197 kV showing overview of needle-like wires broken off from substrate and lying on their  $\{110\}$  faces. Average length from 32 needles was  $1969 \pm 404$  nm (median: 2059 nm). Average width determined from 44 needles was  $144 \pm 11$  nm (median: 141 nm).

faceted sidewalls with an amplitude of roughness of the projected corrugation of the order of  $\sim 3$  nm. Hence, the macroscopic  $\{110\}$  type sidewalls actually form sets of meandering  $\{111\}$  facets, which themselves are atomically flat, as are the top sides of the nanowires. This agrees with the  $\{111\}$  facets having the lowest energy configuration of all facets in the sphalerite structure. Our observation is structurally similar to what has previously been observed for zinc doped GaAs nanowires grown with gold as catalyst [25], although the twin domains in our case are a factor of  $\sim 20$  thinner and the diffraction peaks thus more clearly split.

While the large specimen thickness of 140 nm in figure 5a prevents clear lattice resolution in projection, the  $\sim 1.5$  nm thick amorphous layer visible on the top facet is due to the partial oxidation of the thin GaAsP cap layer mentioned in section 2. Due to the specimen being much thinner near the edges of the hexagonal nanowires, figures 5b and 5c yield much clearer lattice images.

Figure 6 shows a set of annular dark-field (ADF) scanning transmission electron microscopy (STEM) micrographs taken of the same needle at successively higher magnifications. The sampling of the lattice images in figure 6d and 6e was  $7.66$  pm/pixel, and the dumb-bell structure of the  $a/4 = 0.14$  nm lattice spacing between the Ga- and As-columns is well visible in one set of the twins. It is mechanically difficult to orientate an individ-

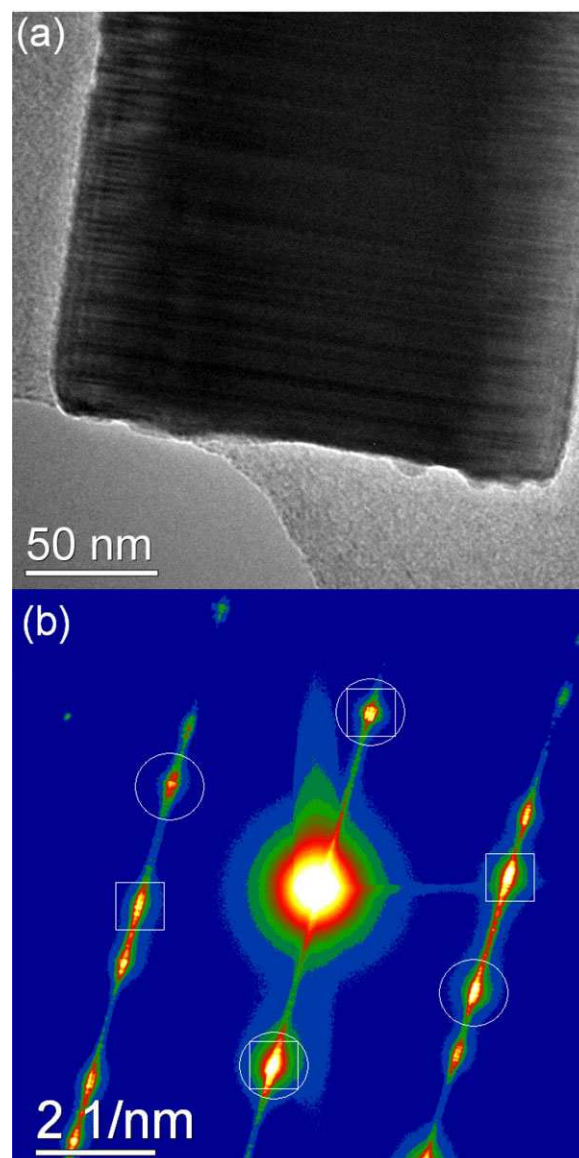


**Fig. 3** (a) BF image of lower end of a typical needle at slightly higher magnification, showing banding, (b) corresponding electron diffraction pattern of same needle (slightly rotated due to the short camera length necessary to record it on the detector placed behind the 3 mm GIF entrance aperture; i.e. this rotation is not a property of the nanowire), demonstrating twinning along the  $\langle 111 \rangle$  growth direction as indicated. The white circles indicate the  $\{111\}$  fringes from one set of twin domains, and the white squares from the other domains. Some of the diffraction peaks are split, due to almost periodical alternation of the twin lamellae.

ual nanowire to better than  $\sim 0.05^\circ$  ( $0.87$  mrad), which geometrically limits the lateral resolution obtainable for a  $\sim 140$  nm thick crystal structure in projection to about  $140 \text{ nm} \times 0.00087 = 0.12$  nm. Due to such residual misalignment of the crystal with respect to the electron

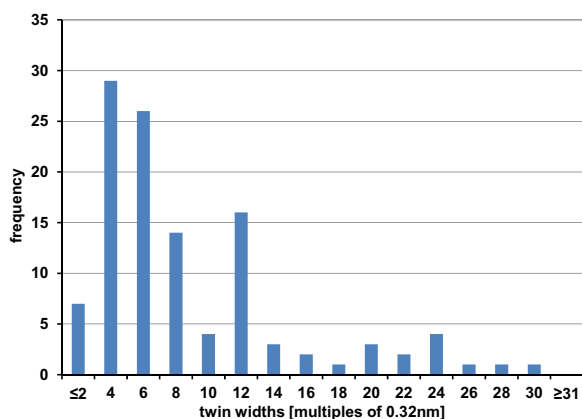


Fig. 4 Histogram of the widths of 144 twins analysed, measured in multiples of  $\{111\}$  lattice planes. Clear maxima occur at 4, 12 and 24, which corresponds to twin domain widths of 1.3, 3.9 and 7.8 nm. The average twin would be only  $2.7 \pm 2.0$  nm thin.

beam direction (near  $\langle 110 \rangle$  zone axis) the corresponding fringe set with 0.14 nm spacing is only visible in one set of twins. Where it is visible, we can clearly distinguish Ga and As atomic columns, and as the latter appear a little brighter than the Ga columns as demonstrated by the linescan in figure 6f, due to the slightly larger atomic number of As (33) compared to Ga (31), we can identify both sub-lattices. This has been done for each of the three twins where the (004) spacing was resolved, and the corresponding atomic structure is overlaid in colour code in the enlarged section of figure 6e. All twins start with a layer of Ga atoms at the bottom and finish with a layer of As atoms at the top, in agreement with the As-termination of the GaAs(111)B substrate used.

We have finally investigated this nanowire by electron energy-loss spectroscopic profiling [26] at 197 kV, employing a round 2 mm entrance aperture in front of the Gatan Imaging Filter (GIF200) fitted below the column of the JEOL 2010F. A rotation holder simplified the vertical orientation of the nanowire so that the twins appeared horizontally on the slow-scan camera detector, as shown in figure 7. Then the GIF was switched to spectroscopy mode, at maximum dispersion. This results in all the intensity passing the spectrometer entrance aperture being dispersed as function of energy line-by-line so that hybrid images are formed, with a spatial coordinate along the vertical  $y$ -direction (here: 0.03 nm/pixel) and energy-loss along the horizontal  $x$ -direction (here: 0.02 eV/pixel) [27]. The twin boundaries are manifest in the lower image of figure 8 as the darker horizontal stripes, and we have extracted sections from that image 15, 35 and 50 pixels high from which we could calculate the electron energy-loss spectra from mostly twinned

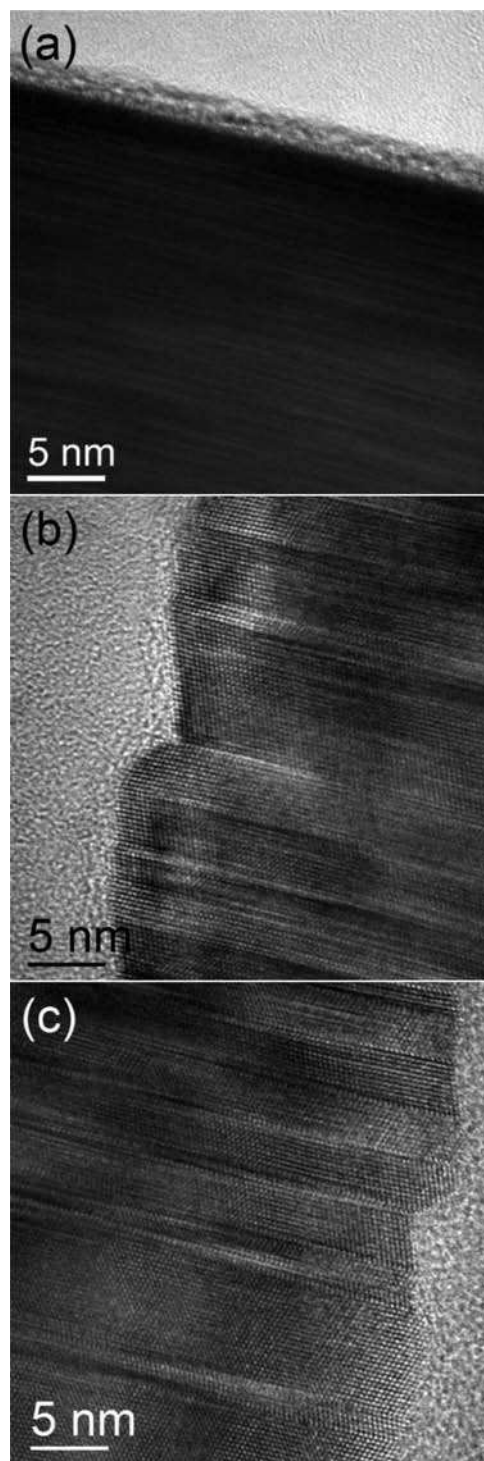


Fig. 5 Set of HREM images depicting the lattice structure of the top facet (a) and two opposite sidewalls (b,c) of a needle. The top is almost atomically flat, the sidewalls are corrugated with  $\{111\}$  type facets that originate from the twins.

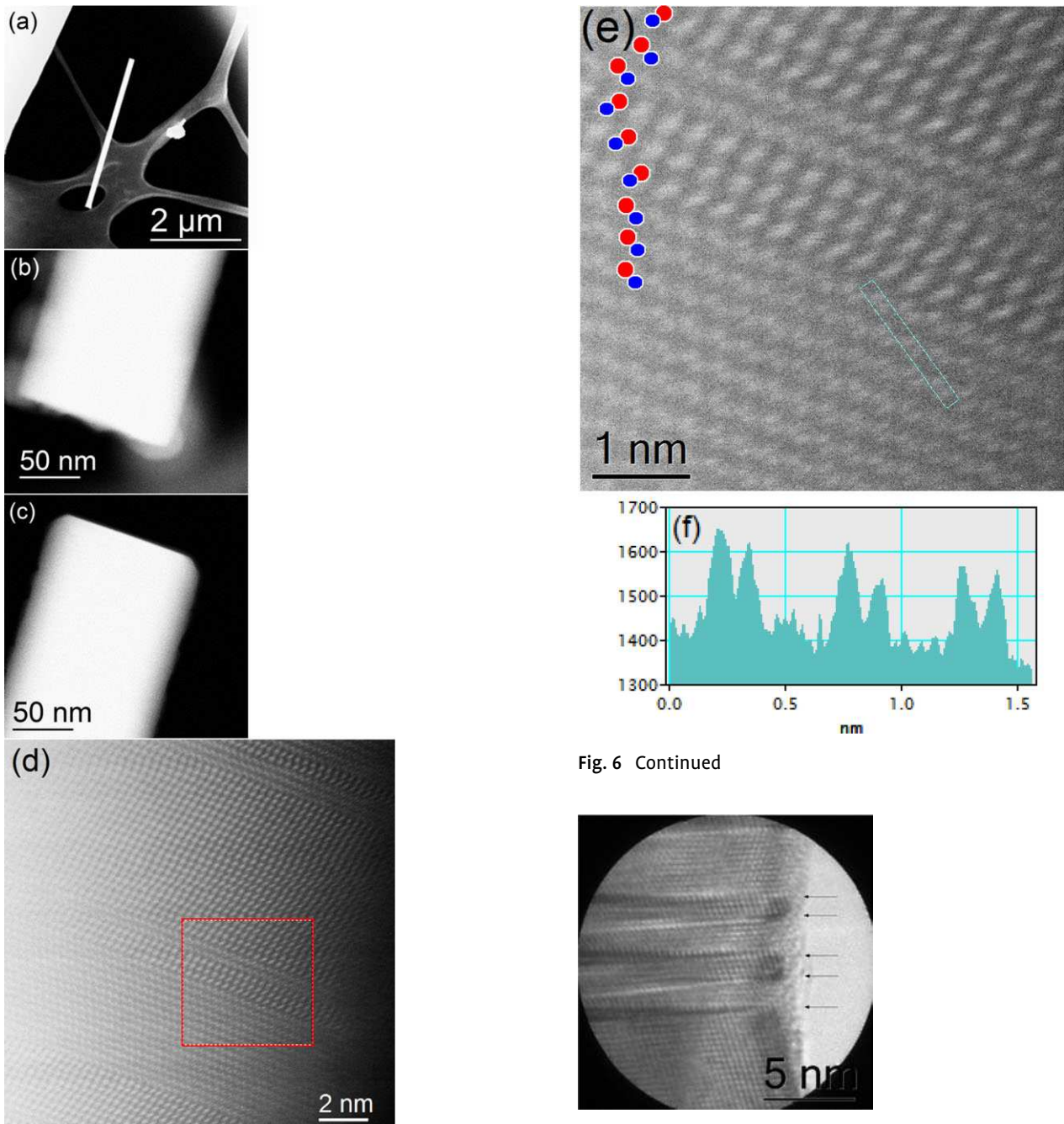


Fig. 6 Continued

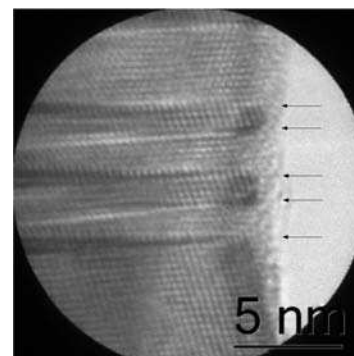
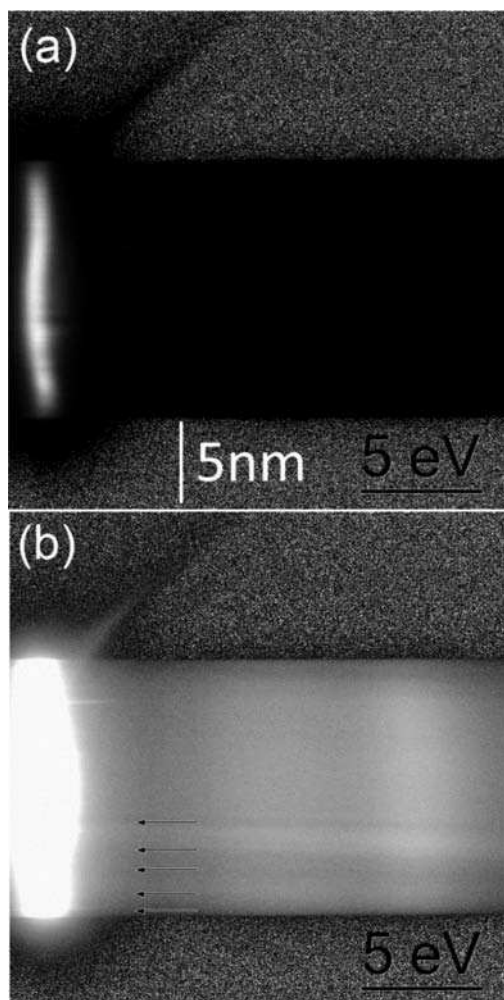


Fig. 7 HREM image at 197 kV and nominal magnification of 80k× with 2 mm spectrometer entrance aperture to the GIF 200 super-imposed. Arrows indicate the positions of five twin boundaries.

Fig. 6 ADFSTEM images acquired at 300 kV of one nanowire which was 3430 nm long (a) and whose bottom (b) and top (c) geometry suggest it has been cut directly above the substrate. No tapering is observed (width at bottom: 139 nm, width hat top: 138 nm). Hence, we know the growth direction of all images points from bottom left towards the top right. The STEM image in (d) shows seven twin boundaries. (e) is an enlarged part of the section marked by a thin red square in (d), with a schematic overlay of As columns (large red circles) and Ga columns (smaller blue circles) to indicate the crystal structure. (f) is an intensity linescan along the rectangular stripe indicated in light blue in (e).

and from bulk sphalerite domains separately, after correction for the non-isochromaticity by aligning the positions of the zero loss peak maximum in each line before vertical summation [28].

The resulting electron energy-loss spectra from bulk GaAs and the twinned GaAs are compared in figure 9. It is clear that both spectra are very similar. The zero



**Fig. 8** Spectroscopic image recorded at 197 kV primary voltage on the JEOL 2010F with nominal 80k $\times$  magnification (to be multiplied by a factor of x19 for the internal magnification of the GIF) and highest dispersion, giving 0.02 eV/pixel along horizontal and 0.03 nm/pixel along the vertical direction. (a) is the spectroscopic image as recorded with 0.5 s exposure where the zero-loss peak appears as an intense stripe near the left side, with an S-type distortion of maximum amplitude  $\sim 0.4$  eV due to the non-isochromaticity of the filter [28]. The extent of the spectroscopic image in height covers  $\sim 600$  of the 1024 detector pixels. (b) shows the same data on a logarithmic scale, with the two vertical bands towards the right representing plasmon losses. The zero-loss now appears saturated. Arrows indicate the positions of the twins visible in figure 7, turned upsidedown at this particular dispersion.

loss peak has a full-width at half maximum of 1.14 eV (bulk sphalerite) and 1.10 eV (twinned GaAs) and, more importantly, a full width at 1/100th of the maximum of 4.14 eV (bulk sphalerite) and 3.56 eV (twin), where the slightly smaller values for the twinned regions may sim-

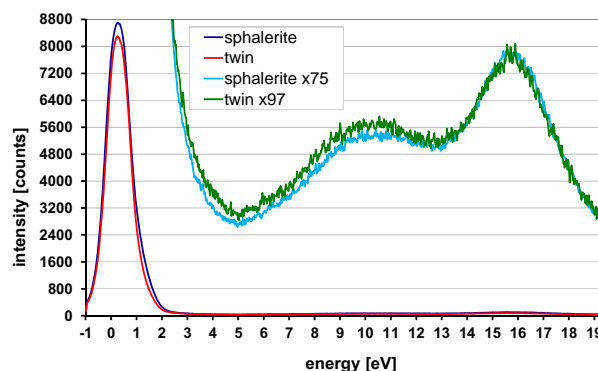


**Fig. 9** EELS spectrum from the regions of bulk GaAs (sphalerite, dark and light blue) and the twinned GaAs (red and, enlarged vertically as indicated, green curve).

ply be due to a slightly better alignment of the spectra extracted. In any case, the base of the zero loss peak is far too wide to allow any conclusion on the band-gap from valence EELS. The volume plasmon peaks at 15.6 eV of both materials are identical (and also identical to tabulated values of 15.7–15.8 eV [29] within the experimental precision of  $\pm 0.1$  eV). However, the smaller peak to the left, which we attribute to a surface/interface plasmon, is slightly more intense near the twin boundary and very slightly shifted (bulk sphalerite:  $10.26 \pm 0.12$  eV, twin:  $10.13 \pm 0.17$  eV). In any case, this shift of 0.13 eV is very small and only detectable by proper curve fitting.

In the future, experiments with novel monochromated field-emission (scanning) transmission electron microscopes may yield less ambiguous results due to improved energy resolution now extending to  $< 50$  meV [30, 31] and improved localisation of the signal due to smaller chromatic tails of the zero loss peak [32]. Even small plasmonic shifts as discussed here may then be measured more reliably and correlated to detailed simulations of the electronic structure of twins associated with the local change of bond symmetry at such twin boundaries.

## 4 Conclusion

We have investigated GaAs nanowires with a quasi-periodic set of rotational twin boundaries by imaging and spectroscopy in (scanning) transmission electron microscopy (STEM/TEM). Atomically resolved STEM imaging revealed the stacking of the cationic sub-lattice and confirmed continuous epitaxial growth of the twins terminating with As-rich surfaces (GaAs(111)B). Spectroscopic profiling indicated a possibly small shift of the interface plasmon energy at the twin boundaries,

which needs to be confirmed by monochromatic EELS measurements with improved energy resolution and smaller tails of the zero loss peak.

**Key words.** GaAs, nanowires, transmission electron microscopy, annular dark field, electron energy-loss spectroscopy.

## References

- [1] M. Koguchi et al., *Jpn. J. Appl. Phys.* **31**, 2061 (1992).
- [2] K. Hiruma et al., *J. Appl. Phys.* **74**, 3162 (1993).
- [3] H. J. Joyce et al., *Nano Lett.* **7**, 921 (2007).
- [4] D. Sparkoska et al., *Phys. Rev. B* **80**, 245325 (2009).
- [5] P. Krogstrup et al., *Nano Lett.* **10**, 4475 (2010).
- [6] Q. H. Xiong, J. Wang, and P. C. Eklund, *Nano Lett.* **6**, 2736 (2006).
- [7] K. A. Dick et al., *Semicond. Sci. Technol.* **25**, 024009 (2010).
- [8] P. Caroff et al., *Nature Nanotechnol.* **4**, 50 (2009).
- [9] T. Akiyama, K. Nakamura, and T. Ito, *Phys. Rev. B* **73**, 235308 (2006).
- [10] H. J. Joyce et al., *Nano Lett.* **10**, 908 (2010).
- [11] X. T. Zhang et al., *Appl. Phys. Lett.* **84**, 2641 (2004).
- [12] H. Okumura, S. Yoshida, and T. Okahisa, *Appl. Phys. Lett.* **64**, 2997 (1994).
- [13] D. E. Lacklison, J. W. Orton, I. Harrison, T. S. Cheng, L. C. Jenkins, C. T. Foxon, and S. E. Hooper, *J. Appl. Phys.* **78**, 1838 (1995).
- [14] U. Bangert, A. Harvey, R. Keyse, and C. Dieker, *Proc. EMAG97 (Cambridge), Inst. Phys. Conf. Ser.* **153**, 273 (1997).
- [15] S. Dhara, P. Magudapathy, R. Kesavamoorthy, S. Kalavathi, K. G. M. Nair, G. M. Hsu, L. C. Chen, K. H. Chen, K. Santhakumar, and T. Soga, *Appl. Phys. Lett.* **87**, 261915 (2005).
- [16] T. Nakamura, Y. Endo, R. Katayama, H. Yaguchi, and K. Onabe, *Phys. Stat. Sol. (c)* **42437**, (2007).
- [17] H. Okumura, S. Misawa, and S. Yoshida, *Appl. Phys. Lett.* **59**, 1058 (1991).
- [18] S. Yoshida, H. Okumura, S. Misawa, and E. Sakuma, *Surf. Sci.* **267**, 50 (1992).
- [19] N. Han, J. J. Hou, F. Y. Wang, S. Yip, H. Lin, M. Fang, F. Xiu, X. L. Shi, T. F. Hung, and J. C. Ho, *Nanoscale Res. Lett.* **7**, 632 (2012).
- [20] A. De and C. E. Pryor, *Phys. Rev. B* **81**, 155210 (2010).
- [21] R. Gurwitz, A. Tavor, L. Karpeles, I. Shalish, W. Yi, G. Seryogin, and V. Narayanamurti, *Appl. Phys. Lett.* **100**, 191602 (2012).
- [22] G. Signorello, E. Lörtscher, P. A. Khomyakov, S. Karg, D. L. Dheeraj, B. Gotsmann, H. Weman, and H. Riel, *Nature Comm.* **5**, 3655 (2014).
- [23] M. N. Makhonin et al., *Nano Lett.* **13**, 861 (2013).
- [24] I. M. Ross and T. Walther, *Proc. EMAG 2011, Birmingham, UK (IoP Publishing, Bristol) J. Phys. Conf. Ser.* **371**, 012012 (2012).
- [25] T. Burgess, S. Breuer, P. Caroff, J. Wong-Leung, Q. Gao, H. H. Tan, and C. Jagadish, *ACS Nano* **7**, 8105 (2013).
- [26] T. Walther and W. Mader, *Proc. Microsc. Semicond. Mater. Conf. (Oxford) Inst. Phys. Conf. Ser.* **164**, 121 (1999).
- [27] T. Walther, *Z. Metallkd.* **96**, 429 (2006).
- [28] T. Walther, *Ultramicroscopy* **96**, 401 (2003).
- [29] R. F. Egerton, *Electron Energy-Loss Spectroscopy in the Electron Microscope 2nd edition (Plenum, New York, 1996)*, p. 432.
- [30] E. Essers, G. Benner, T. Mandler, S. Meyer, D. Mittmann, M. Schnell, and R. Höschel, *Ultramicroscopy* **110**, 971 (2010).
- [31] O. L. Krivanek, T. C. Lovejoy, N. Dellby, and R. W. Carpenter, *Microscopy* **62**, 3 (2013).
- [32] T. Walther, E. Quandt, H. Stegmann, A. Thesen, and G. Benner, *Ultramicroscopy* **106**, 963 (2006).